

Accepted, 8 Sept. 2011

# *Fermi*/LAT Observations of *Swift*/BAT Seyferts: on the Contribution of Radio-quiet AGN to the Extragalactic $\gamma$ -ray Background

Stacy H. Teng <sup>1,2,3</sup>, Richard F. Mushotzky <sup>2</sup>, Rita M. Sambruna <sup>4</sup>, David S. Davis <sup>3,5</sup>, and Christopher S. Reynolds <sup>2</sup>

## ABSTRACT

We present the analysis of 2.1 years of *Fermi*/LAT data on 491 Seyfert galaxies detected by the *Swift*/BAT survey. Only the two nearest objects, NGC 1068 and NGC 4945, which were identified in the *Fermi* First-year Catalog, are detected. Using the *Swift*/BAT and radio 20 cm fluxes, we define a new radio-loudness parameter  $R_{X,BAT}$  where radio loud objects have  $\log R_{X,BAT} > -4.7$ . Based on this parameter, only radio loud sources are detected by *Fermi*/LAT. An upper limit to the flux of the undetected sources is derived to be  $\sim 2 \times 10^{-11}$  photons cm<sup>-2</sup> s<sup>-1</sup>, approximately seven times lower than the observed flux of NGC 1068. Assuming a median redshift of 0.031, this implies an upper limit to the  $\gamma$ -ray (1–100 GeV) luminosity of  $\lesssim 3 \times 10^{41}$  erg s<sup>-1</sup>. In addition, we identified 120 new *Fermi*/LAT sources near the *Swift*/BAT Seyferts with significant *Fermi*/LAT detections. A majority of these objects do not have *Swift*/BAT counterparts, but their possible optical counterparts include blazars, FSRQs, and quasars.

## 1. Introduction

Recently, the *Fermi*/Large Area Telescope (LAT) team has released the first year catalog of LAT-detected active galactic nuclei (AGNs) with greater than 5- $\sigma$  significance

---

<sup>1</sup>Contacting author: stacyt@astro.umd.edu.

<sup>2</sup>Department of Astronomy, University of Maryland, College Park, MD 20742, U.S.A.

<sup>3</sup>CRESST and X-ray Astrophysics Laboratory, NASA/GSFC, Greenbelt, MD 20771, U.S.A.

<sup>4</sup>Department of Physics and Astronomy, George Mason University, Fairfax, VA 22030, U.S.A.

<sup>5</sup>Department of Physics, University of Maryland Baltimore County, Baltimore, MD 21250, U.S.A.

(Abdo et al. 2010a). Along with many blazars and several radio galaxies, a few Seyfert galaxies (specifically NGC 1068 and NGC 4945), traditionally classified as radio-quiet sources, are listed as possible counterparts to the *Fermi*/LAT sources. Foschini et al. (2011) also reported the *Fermi*/LAT detection of  $\gamma$ -ray emission from the narrow-line Seyfert 1 galaxy PMN J0948+0022. The detection of type-1/2 AGN at GeV energies represents a major breakthrough for *Fermi*, as it points to a new class of  $\gamma$ -ray emitters. Observationally, this is an exciting discovery as no Seyfert was previously detected with EGRET. The canonical spectral energy distribution (SED) of a radio-quiet AGN has a turnover around several hundred keV (e.g., Dermer & Gehrels 1995); GeV  $\gamma$ -ray emission is usually not part of our standard view of these systems. However, there are theoretical reasons to expect significant  $\gamma$ -ray emission from the active nucleus of Seyferts of all luminosities, and depending on their  $\log N - \log S$ , Seyferts could turn out to be non-negligible contributors to the extragalactic  $\gamma$ -ray background (EGB), contrary to current claims (Ajello et al. 2009).

From a theoretical point of view,  $\gamma$ -ray emission from the active nucleus in Seyferts is not unexpected. At sub-Eddington luminosities, it is quite likely that accretion proceeds via radiatively inefficient flows (e.g., ADAF; Narayan & Yi 1994). Here, electrons are heated to temperatures  $T_e \sim 10^9$  K via interactions with protons of  $T_p \sim 10^{12}$  K, and produce the observed radiation via bremsstrahlung and inverse Compton scattering of the disk optical-IR photons, producing a bump from IR to X-rays with hard X-ray continua. A general feature of ADAF models is that they predict a second bump peaking around  $10^{23}$  Hz due to the decay of pions produced in the collisions of the hot proton gas (e.g., Mahadevan et al. 1997; Oka & Manmoto 2003). The exact shape and normalization of the  $\gamma$ -ray peak are a function of a number of parameters, including the black hole spin, since for larger values of the spin the disk extends deeper in the gravitational well with higher proton temperatures and hence higher X-to- $\gamma$ -ray flux ratios. For high spin values ( $a=0.95$ ) and favorable values of the other parameters, the X-to- $\gamma$ -ray flux ratio  $\sim 1$ . The peak emission is near 100 MeV and decreases very sharply with energy in models without non-thermal protons. Thus, by measuring the *Fermi*/LAT flux and, possibly, the spectrum, it is possible to constrain several important quantities in the ADAF, e.g., the black hole spin and the gas composition.

Another possible scenario for  $\gamma$ -ray emission in radio-quiet sources may be due to coronal effects. At higher luminosities ( $\sim 1\%$  Eddington or larger), the conventional view is that the X-rays are produced via inverse Comptonization of soft (UV/optical) photons from a radiatively-efficient accretion disk by electrons in a hot disk corona. The corona is believed to be heated by magneto-hydrodynamic (MHD) waves or magnetic reconnection associated with MHD turbulence in the underlying disk (e.g., Miller & Stone 2000). While the corona is normally treated as a thermal plasma with temperature 100–200 keV, the corona is likely to be a marginally collisionless plasma (Goodman & Uzdensky 2008) and this raises the

possibility that non-thermal particle acceleration may accompany the magnetic heating. The detection of a hard  $\gamma$ -ray tail beyond the “thermal cutoff” of the X-ray spectrum would be strong evidence for a population of non-thermal accelerated electrons within the corona.

Finally, the  $\gamma$ -ray emission may be produced by interactions between possible jets and the immediate environment of the active nucleus. Some Seyferts with deep radio imaging do exhibit parsec-scale ejecta, similar to radio-loud sources (e.g., Nagar et al. 2001). An example is NGC 1068, a type-2 source with a parsec-scale radio jet interacting with a molecular cloud near the nucleus (Gallimore et al. 2004). While the jets are in general only mildly relativistic, and beaming is not strong enough to amplify non-thermal  $\gamma$ -ray emission, the jet-ISM interaction could in principle be responsible for the production of  $\gamma$ -rays via hadronic processes (proton-proton collisions), as observed in starbursts.

The *Swift*/BAT sample of nearby Seyfert galaxies consists of non-blazars detected with *Swift*/BAT in the 14–195 keV energy range. In the following section, we will discuss the *Swift*/BAT sample and our *Fermi* data analysis. In § 3, we will discuss the results and their implications; a summary of our findings is presented in § 4. Throughout the rest of this paper, we assume the cosmology  $H_0 = 71 \text{ km s}^{-1} \text{ Mpc}^{-1}$ ,  $\Omega_M = 0.27$ , and  $\Omega_\Lambda = 0.73$ . The *Fermi* flux will be measured in the 1–100 GeV energy band where the effective area of *Fermi*/LAT is the highest.

## 2. Sample Selection and *Fermi*/LAT Data Analysis

### 2.1. The *Swift*/BAT Sample of Seyferts

The Burst Alert Telescope (BAT) on board *Swift* operates in the 14–195 keV energy range and with a field of view of  $\sim 10\%$  of the sky. BAT observes 60% of the sky on average each day at the 20 mCrab level. After 58 months of operation, the *Swift*/BAT catalog has identified 519 Seyfert galaxies and 108 beamed AGN sources in addition to many pulsars, X-ray binaries, and other classes of objects (Baumgartner et al. 2010)<sup>1</sup>. Hard X-ray sources are identified in the BAT survey with position localizations of about  $4'$ . These positions were checked against the archives of X-ray telescopes with high spatial resolution like *Chandra* and *XMM-Newton* in order to identify an X-ray counterpart to the BAT source. Sources with no historical observations were observed with *Swift*/XRT in order to identify a counterpart.

The BAT Seyfert sample is ideal for our study. These sources are nearby, thus maxi-

---

<sup>1</sup><http://heasarc.gsfc.nasa.gov/docs/swift/results/>

mizing the likelihood of being bright at  $\gamma$ -rays. The redshift distribution of the *Swift*/BAT Seyferts is highly biased towards  $z \sim 0.03$ . Since BAT is insensitive to the effects of dust and Compton-thin obscuration, the BAT AGN sample can be considered an uniform and complete flux-limited sample of AGN in the local Universe. The sample includes classical objects that are well-studied at other wavelengths as well as relatively less well-known sources. Currently, there is an active program to obtain imaging and spectroscopic data at infrared, optical, and X-rays (Winter et al. 2010, and references therein). Archival VLA data are also available through NVSS (Condon et al. 1998) and FIRST (White et al. 1997) for most of these sources.

## 2.2. Catalog Matching

The initial *Fermi*/LAT Seyfert sample was selected by cross-correlating the positions from the 58-month *Swift*/BAT catalog (Baumgartner et al. 2010) with those from the 11-month *Fermi*/LAT Point Source Catalog (PSC). The PSC dictates that the sources must be detected with a minimum signal-to-noise of  $4\sigma$ . The criterion for a positional match was set to be within 10 arcminutes. Of the 1099 *Swift*/BAT sources, 81 objects were matches between the *Swift*/BAT and *Fermi*/LAT catalogs. After the exclusion of obvious non-AGN objects such as neutron stars, pulsars, local starbursts, objects with unknown redshifts, and those without prior identifications, we reduced the total number of objects to 53. Of these, a majority are known blazars. We further reduced our sample to a total of five objects that are not blazar candidates (e.g., Healey et al. 2008; Massaro et al. 2009). Only two of these sources have optical counterparts within the *Fermi*/LAT error circle. These are NGC 1068 and NGC 4945.

Both *Fermi*/LAT and *Swift*/BAT have large fields of view and the errors associated with source positions are therefore large. We performed Monte Carlo simulations to determine the rate of false matches between the two catalogs. We randomized the *Swift*/BAT catalog positions by adding or subtracting a random number greater than 10 arcminutes (our positional match criterion) to the right ascension and declination from the *Swift*/BAT data. The randomized *Swift*/BAT positions are then matched to the *Fermi*/LAT PSC positions. Assuming no contamination from sources in the Galactic disk, the average random matches between the two catalogs is 3.3 from 100 simulations. This implies that there is  $\sim 4\%$  (3.3 out of 81 matches) false match rate between the two catalogs.

### 2.3. Data Reduction

To potentially extend the number of *Fermi* detections, we analyzed  $\sim 2.1$  years of *Fermi*/LAT data in the 1–100 GeV energy range for our sample, spanning from August 4, 2008 to September 2, 2010. The data reduction was performed using the *Fermi Science Tools* version v9r15p2. We followed the *Fermi*/LAT data analysis threads provided by the Fermi Science Support Center (FSSC)<sup>2</sup>. In particular, we used the P6V3 instrument response. Using the more extensive 2-year data, we determined the detection significance of the objects based on binned likelihood analysis. Again, only two objects, NGC 1068 and NGC 4945, are detected by *Fermi*/LAT with significant signal to noise ratios and have optical counterparts within the positional error circle. The general properties of these two sources and modeling statistics are listed in Table 1.

While 519 Seyferts were identified in the 58-month catalog, 28 were classified as such based on X-ray spectra and not the traditional optical methods. Therefore, only 491 Seyferts from the *Swift*/BAT catalog were considered in our analysis due to uncertain classifications. For fields centered on 276 of the 491 Seyferts, we find that the likelihood analysis is unable to successfully fit all of the  $\gamma$ -ray photons. These fields are associated with very luminous  $\gamma$ -ray objects (e.g., 3C 273 and 3C 279) and were eliminated from subsequent analysis because the contaminating flux at the target position introduced unacceptably large uncertainties in the target flux estimates. For the remaining 215 fields, we measured the fluxes of the undetected sources using the binned likelihood analysis. Given the position of the *Swift*/BAT source, we assumed a  $\gamma$ -ray photon index of 2.4 for the input power law model to estimate the flux for a point source as if the galaxy were detected. The value of 2.4 was assumed because this is the spectral index of the *Fermi*/LAT background after the removal of the resolved sources (Abdo et al. 2010b); if the Seyferts make up the unresolved background, their individual spectral shapes must approximate the shape of the total spectrum. The assumed spectral index is also consistent with the measured spectral indices of NGC 1068 and NGC 4945 (Table 1). Figure 1 shows the distribution of these derived fluxes. The distribution of the measured fluxes appear to follow a narrow Gaussian distribution centered at zero with  $\sigma$  of  $\sim 1 \times 10^{-10}$  photons cm<sup>-2</sup> s<sup>-1</sup>. The negative values are due to variations in the background from both instrumental noise and the accuracy of the background model.

---

<sup>2</sup><http://fermi.gsfc.nasa.gov/ssc/data/analysis/scitools/>.

## 2.4. Stacking Analysis

Following the individual source analysis, we performed a stacking analysis for objects with non-detections. This allows us to determine an upper limit to the  $\gamma$ -ray flux of the *Swift*/BAT Seyferts. An updated version (v9r18p6) of the *Fermi Science Tools* released in November 2010 was used for this analysis. We modified the Python script for composite likelihood to apply an assumed model to all of the fields simultaneously with a single model. The script starts with the “best-fit” model of each field centered on a BAT source from the individual analysis and an inferred model for the Seyfert of interest. This upper limit model is linked to be the same for all targets. For this, we assume a power law with a fixed  $\Gamma = 2.4$  and only allow the flux (normalization) value to vary. The upper limit is determined when the  $\Delta$ TS value from the composite likelihood is 2.706 for one degree of freedom (at the 90% confidence level).

The stacking analysis estimates the upper limit to be  $\sim 2 \times 10^{-11}$  photons  $\text{cm}^{-2} \text{s}^{-1}$  in the *Fermi* band, approximately five times lower than the  $1-\sigma$  of the distribution from individual analysis (Figure 1). The stacking upper limit corresponds to an energy flux of  $\sim 9 \times 10^{-14}$  ergs  $\text{cm}^{-2} \text{s}^{-1}$ . Assuming the median redshift of the 215 stacked objects ( $z \sim 0.031$ ), this implies a *Fermi*/LAT luminosity limit of  $\sim 3 \times 10^{41}$  ergs  $\text{s}^{-1}$ . This is approximately 3 and 18 times the *Fermi*/LAT luminosities of NGC 1068 and NGC 4945, respectively, the nearest known Seyferts in the *Swift*/BAT sample (Table 1). Thus, the lack of detection of more distant Seyferts is likely a sensitivity issue.

## 2.5. New *Fermi*/LAT Sources

From the individual fits, we have identified 120 new extragalactic *Fermi*/LAT sources with significant detections ( $\sigma > 4$ ) in the fields of the *Swift*/BAT sample (Table 2). These sources were not included in the PSC. The optical counterparts of these objects were identified as objects within 10 arcminutes of the nominal *Fermi*/LAT positions. When objects have multiple counterparts within the error circle, the one with a radio counterpart and the brightest is selected. A majority of these 120 new sources have optical counterparts that are previously identified as quasars, flat-spectrum radio quasars (FSRQs), or BL Lac objects. Only 17 of these have *Swift*/BAT counterparts; all but one has *Swift*/BAT detection threshold below  $\sigma < 4$  (a selection criterion for the 58-month catalog). The fact that these blazars were undetected by *Swift*/BAT is consistent with luminous blazars being brighter in  $\gamma$ -ray than hard X-ray (e.g., Sambruna et al. 2010).

### 3. Discussion

#### 3.1. Starburst Contribution

While the current article aims to address the contribution of radio quiet AGNs to the EGB, it should be noted that starbursts may also contribute to the  $\gamma$ -ray output. Lenain et al. (2010) suggested that a starburst contributes significantly to the  $\gamma$ -ray luminosity of NGC 4945. From their analysis, NGC 4945 falls on a linear relationship between the supernova rate, the total gas mass, and the  $\gamma$ -ray luminosity along with M 82, NGC 253, the Large Magellanic Cloud, and the Milky Way. However, the higher detection rate of starbursts as compared to Seyferts by *Fermi*/LAT does not necessarily imply starbursts are bigger contributors to the EGB than active nuclei. Given the high dependence of detection on the intrinsic  $\gamma$ -ray luminosity and the distance of the objects, radio quiet AGNs may simply be harder to detect because there are more nearby starbursts than Seyferts. We can set an upper limit on the detectability of a pure starburst galaxy at the median distance of the *Swift*/BAT Seyferts by scaling the  $\gamma$ -ray luminosity upper limit by that of M 82 ( $\sim 4 \times 10^{40}$  erg s $^{-1}$ ). This indicates that the star formation rate cannot be more than about 7 times what is currently seen in M 82, or else it would already have been detected. The corresponding upper limit on the star formation rate necessary to produce this level of  $\gamma$ -ray emission is 45 M $_{\odot}$  per year. This star formation rate is far higher than the typical range seen in Seyfert galaxies (SINGS; Smith et al. 2007). Thus, it is unlikely for star formation to be the only, or even major, source of  $\gamma$ -ray emission in these galaxies.

#### 3.2. Radio Loudness

In the third scenario for  $\gamma$ -ray production outlined in § 1 where the jets from the AGN interact with its local environment, these sources are expected to be radio-loud. The classical way of measuring radio loudness is that of Kellerman et al. (1989), by the radio-to-optical luminosity ratio ( $R_o$ ). By their definition, radio loud objects have radio luminosities at 5 GHz ten times that of their B-band luminosities, or  $R_o > 10$ . However, Terashima & Wilson (2003) noted that optical observations may be subject to obscuration and thus  $R_o$  may be over estimated for some objects. For many galaxies, the large optical apertures may also include contributions from stellar light, thus underestimating  $R_o$ . Since X-ray (2–10 keV) observations are less likely to be affected by dust, Terashima & Wilson (2003) defined  $R_X$ , the radio-to-2–10 keV luminosity ratio, as their measure of radio loudness. Based on their study, radio loud objects have  $\log R_X > -4.5$ . This is consistent with the  $R_X$  boundary ( $\log R_X > -4.3$ ) established by La Franca et al. (2010) using data from 1600 AGNs.

For objects with very high column densities ( $N_H \sim 10^{24} \text{ cm}^{-2}$ ), even the 2–10 keV luminosity can be suppressed. Thus,  $R_X$  for Compton-thick, or nearly Compton-thick, sources may be inaccurate. At above 10 keV, absorption is less likely to affect the X-ray measurements. We therefore use the 14–195 keV *Swift*/BAT measurements to define  $R_{X,BAT} = L_{1.4\text{GHz}}/L_{X,BAT}$  and to determine radio loudness. To establish the boundary between radio-loud and radio-quiet objects in  $R_{X,BAT}$ , we first determined the distribution of  $R_{X,BAT}$  for Seyfert 1.0s. From the *Swift*/BAT sample, there are 169 galaxies classified as Seyfert 1.0s. These objects are the least likely to have obscuration in the line of sight. Of these, 31 have high resolution 1.4 GHz measurements from the FIRST survey. The FIRST images confirm that these Seyfert 1.0 sources do not have any extended radio emission. The range of  $\log R_{X,BAT}$  for the Seyfert 1.0s is between  $-6.3$  and  $-4.7$ , with a median value of  $-5.7$ .

Given the observed range in  $R_{X,BAT}$  parameters, what is the cut-off for radio-loudness? The La Franca et al. (2010) results suggest the  $\log R_X -4.3$  boundary. Of the 31 Seyfert 1.0s with FIRST fluxes, seven have published 2–10 keV fluxes. For unabsorbed sources such as these, a direct relationship between the *Swift*/BAT and 2–10 keV fluxes is expected. A linear regression analysis comparing the *Swift*/BAT and 2–10 keV fluxes for all seven sources results in a correlation coefficient of  $R^2 = 0.09$ , suggesting no correlation even for these unobscured sources. However, after the removal of a single outlier (NGC 985, a ring galaxy), the correlation improves to  $R^2 = 0.95$ , consistent with expectation albeit with a small number of objects. The data imply

$$f_{2-10 \text{ keV}} = 0.42 f_{BAT}. \quad (1)$$

This relationship is approximately that assumed by Rigby et al. (2010), who used the conversion  $f_{2-10 \text{ keV}} = 0.37 f_{BAT}$  derived from AGN spectral templates constructed by Marconi et al. (2004). Using our empirical relation, the  $\log R_{X,BAT}$  values for the 31 Seyfert 1.0s correspond to  $\log R_X$  where  $\log R_X \sim \log R_{X,BAT} + 0.4$ . The empirical relation is approximately consistent with a power law model with a photon index of 1.7. Therefore, using the La Franca et al. (2010) cut-off, we define an object to be radio loud if

$$\log \frac{f_{1.4 \text{ GHz}}}{f_{BAT}} > -4.7. \quad (2)$$

The advantage of using  $R_{X,BAT}$  as the radio loudness selection over  $R_X$  is clearly demonstrated in NGC 4945. A well-known Compton-thick object, its  $\log R_X$  value ( $-3.6$ ) places it well into the radio loud category whereas its  $\log R_{X,BAT}$  value ( $-4.3$ ) puts it near the cutoff.

Figure 2 shows the distribution of  $\log R_{X,BAT}$  for the extragalactic *Swift*/BAT sources from the 58-month catalog. The distribution is skewed toward the radio quiet sources, but it



is not necessarily an accurate representation of the complete sample because it depends on the availability of reliable radio data. The two *Fermi*-detected sources appears to be two of the most radio-loud objects in the *Swift*/BAT sample, very similar to the  $\log R_{X,BAT}$  range of blazars and FSRQs detected by *Fermi*/LAT. Nearly all of the radio loud objects from the *Swift*/BAT catalog have already been detected by *Fermi*.

### 3.3. Implications for the EGB

Blazars (BL Lac objects and FSRQs) are known to contribute to about 16% of the EGB at above 100 MeV (Abdo et al. 2010b)<sup>3</sup>; the origin of the remaining fraction is still a mystery. Radio quiet AGNs like Seyfert galaxies, though intrinsically faint, may turn out to be a significant source of the EGB if there is a large number of Seyferts. Using *Swift*/BAT data, Ajello et al. (2009) concluded that blazars, specifically FSRQs, begin to dominate the cosmic X-ray background (CXB) above a few hundred keV. Seyfert galaxies dominate the CXB at below this energy and in the *Swift*/BAT energy band (Gilli et al. 2007). Thus, a relatively high  $\gamma$ -to-X-ray flux ratio may imply radio quiet AGNs are a significant source of the EGB (assuming no cosmic evolution).

Figure 3 shows the distribution of the upper limits of the  $\gamma$ -to-X-ray flux ratio of the *Fermi*-undetected sources. The EGB/CXB ratio as derived from *Fermi* 1–100 GeV data (Abdo et al. 2010c) and *Swift* data (Ajello et al. 2008) is 1.2% which is above the limits placed on the  $\gamma$ -to-X-ray flux ratios by *Fermi*/LAT. Therefore, the radio quiet Seyferts are not a significant source of the EGB. The  $\gamma$ -to-X-ray flux ratio distribution also suggests that inefficient accretion flow around a black hole with a high spin value is not a viable mechanism for  $\gamma$ -ray emission (see § 1) as the model suggests an observed  $\gamma$ -to-X-ray flux ratio of unity.

The cumulative  $\log N - \log S$  in Figure 4 suggests that the *Swift*/BAT Seyferts would only begin to dominate the EGB over the blazars at very low flux levels ( $\lesssim 10^{-12}$  photons  $\text{cm}^{-2} \text{s}^{-1}$ ) if we assume Seyferts in fact produce  $\gamma$ -rays. This limit is far below the current sensitivity of *Fermi* data (about ten times below our upper limit). In the 1–100 GeV band, blazars actually only contribute to  $\sim 16.6\%$  of the EGB intensity (Abdo et al. 2010b). If we assume that Seyferts make up the rest of the EGB intensity and follow the  $\log N - \log S$  relation derived from *Swift*/BAT data, then it would require the ability to detect individual sources at the  $\lesssim 10^{-23}$  photons  $\text{cm}^{-2} \text{s}^{-1}$  level for the integrated flux to equal that of the

---

<sup>3</sup>The estimate of 16% contribution from blazars given in Abdo et al. (2010b) is the fraction relative to the unresolved *Fermi*/LAT background rather than the total EGB. Ghirlanda et al. (2011) and Inoue et al. (2009) estimate that blazars contribute to  $\sim 45\%$  of the total EGB.

“missing”  $\gamma$ -ray background, far below the source confusion level of *Fermi* at 1 GeV. The contribution of the Seyferts are so small that it would necessitate the detection of a large number of these faint sources to make up the background. Conversely, at the confusion limit of *Fermi*/LAT at 1 GeV, the limiting flux is  $\lesssim 1 \times 10^{-12}$  photons  $\text{cm}^{-2} \text{s}^{-1}$ , assuming the same  $\log N - \log S$  slope. As *Fermi* continues to scan the  $\gamma$ -ray sky, it may be possible to identify  $\gamma$ -ray emission from radio quiet AGNs near the end of the nominal lifetime of *Fermi* ( $\sim 10$  years).

#### 4. Summary

From our analysis of 2.1 years of *Fermi*/LAT data on 491 Seyfert galaxies selected from the 58-month *Swift*/BAT catalog, we derived upper limits to the  $\gamma$ -ray flux and luminosity of radio quiet AGNs. We defined a new radio loudness parameter ( $\log R_{X,BAT}$ ) which confirms that only radio loud objects have been isolated and identified by *Fermi*. The cumulative  $\log N - \log S$  of the *Swift*/BAT Seyferts suggests that radio quiet AGNs would only begin to dominate the EGB over blazars at a flux level of  $\lesssim 10^{-12}$  photons  $\text{cm}^{-2} \text{s}^{-1}$ .

We are grateful to the referee for providing insightful comments that improved the manuscript. We thank Wayne Baumgartner and the *Swift*/BAT team for providing the BAT 58 month catalog ahead of its release. We made use of the NASA/IPAC Extragalactic Databased (NED), which is operated by the Jet Propulsion Laboratory, Caltech, under contract with NASA. We acknowledge support by NASA through the *Fermi* General Observer Program.

#### REFERENCES

- Abdo et al. 2009, ApJ, 707, L142
- Abdo et al. 2010a, ApJ, 715, 429
- Abdo et al. 2010b, ApJ, 720, 435
- Abdo et al. 2010c, Phys. Rev. Letter, 104, 101101
- Ajello et al. 2008, ApJ, 689, 666
- Ajello et al. 2009, ApJ, 699, 603

- Baumgartner, W.H. et al. 2010, ApJS, submitted
- Condon, J.J. et al. 1998, AJ, 115, 1693
- Dermer, C.M. & Gehrels, N. 1995, ApJ, 447, 103
- Foschini, L. et al. 2011, MNRAS, 413, 1617
- Gallimore, J.F., Baum, S.A., & O’Dea, C.P. 2004, ApJ, 613, 794
- Ghirlanda, G., Ghisellini, G., Tavecchio, F., Foschini, L., & Bonnoli, G., 2011, MNRAS, 413, 852
- Gilli, R., Comastri, A., & Hasinger, G. 2007, A&A, 463, 79
- Goodman & Uzdensky 2008, ApJ, 682, 608
- Healey, S.E. et al. 2008, ApJS, 175, 97
- Inoue, Y. et al. 2009, in Proc. Fermi Symp., preprint (arXiv:1001.0103)
- Kellerman, K.I. et al. 1989, AJ, 98, 1195
- La Franca, F., Melini, G., & Fiore, F. 2010, ApJ, 718, 368
- Lenain et al. 2010, A&A, 524, A72
- Mahadevan et al. 1997, ApJ, 486, 268
- Marconi, A. et al. 2004, MNRAS, 351, 169
- Markoff et al. 2005, ApJ, 635, 1203
- Massaro, E. et al. 2009, A&A, 495, 691
- Miller & Stone 2000, ApJ, 534, 398
- Nagar, N.M., Wilson, A.S., & Falke, H. 2001, ApJ, 559, 87L
- Oka & Manmoto 2003, MNRAS, 340, 543
- Narayan & Yi 1994, ApJ, 428, 13L
- Rigby, J.R., Diamond-Stanic, A.M., & Aniano, G. 2009, ApJ, 700, 1878
- Sambruna, R.M. et al. 2010, ApJ, 710, 24

Smith, B.J. et al. 2007, AJ, 133, 791

Terashima, Y. & Wilson, A.S. 2003, ApJ, 583, 145

White, R.L. et al. 1997, AJ, 475, 479

Winter, L.M. et al. 2010, ApJ, 710, 503

---

This preprint was prepared with the AAS L<sup>A</sup>T<sub>E</sub>X macros v5.2.

Table 1. The Sample

<i>Fermi</i> /LAT ID (1)	Association (2)	$z$ (3)	Type (4)	S/N (5)	D <sub>L</sub> (6)	$\Gamma$ (7)	L <sub><math>\gamma</math></sub> (8)	log $R_{X,BAT}$ (9)
1FGL J0242.7+0007	NGC 1068	0.004	Sy 2	9.1	12.6	2.35±0.12	$1.0 \times 10^{41}$	−3.7
1FGL J1305.4−4928	NGC 4945	0.002	Sy 2	11.4	11.1	2.32±0.08	$1.7 \times 10^{40}$	−4.3

Note. — Col.(1): *Fermi*/LAT source identifier. Col.(2): Source association. Col.(3): Redshift. Col.(4): Optical spectral type, from NED. Col.(5): Approximate detection significance ( $\sigma$ ) in the 100 MeV – 300 GeV range from the 2-year *Fermi*/LAT data. Col.(6): Luminosity distance in Mpc derived relative to the reference frame defined by the 3K Microwave Radiation Background (e.g., NED). Col.(7): Photon index in the 1–100 GeV energy range as derived from *Fermi*/LAT data. Col.(8):  $\gamma$ -ray luminosity in units of ergs cm<sup>−2</sup> s<sup>−1</sup> in the 1–100 GeV energy range. Col.(9): log  $R_{X,BAT}$ .

Table 2. Non-BAT Sources

RA (1)	Dec (2)	Sign. (3)	OptID (4)	BAT? (5)	Comments (6)
11.3971	−37.2896	7.9	[VCV96] Q0042−3734 (5′7)	...	Quasar at z=2.1
11.4565	12.1716	7.2	RX J0045.6+1217 (7′1)	2.0	X-ray source with radio and IR counterparts
11.6186	11.9891	4.5	1RXS J004700.8+115827 (8′0)	...	X-ray source
14.0353	−21.2382	7.0	2MASX J00561157−2109221 (3′0)	...	Unknown galaxy type
17.5903	61.4336	19.4	NVSS J010953+612231 (4′8)	...	Radio source
21.2783	−22.8700	6.6	GALEX 2674762193050796919 (4′9)	...	Possible quasar
21.4997	−25.9199	4.4	2dFGRS S148Z245 (2′6)	...	Galaxy of unknown type at z=0.11
22.0088	−8.2834	4.7	MCG−02−04−055 (6′8)	...	Galaxy of unknown type at z=0.023
28.3368	1.5573	7.0	2MASX J01525339+0127497 (7′7)	3.0	IR source and X-ray source
31.6304	−11.8300	9.7	CGRaBSJ0206−1150 (1′5)	...	FSRQ
34.5728	18.3418	5.4	IRAS F02150+1808 (7′2)	...	IR source
34.8650	36.5856	7.8	V Zw 217 (0′6)	...	Galaxy of unknown type
39.0939	−61.9344	4.0	2dFGRS S913Z520 (1′4)	...	Galaxy of unknown type
43.8035	32.1962	4.4	B2 0252+32 (9′4)	...	Radio source
47.3045	10.5395	12.5	PKS J0309+1029 (3′9)	...	FSRQ
50.6060	−37.4430	5.2	ESO 301−G 008 (2′7)	...	Starburst, a dS0 in cluster
51.8087	−15.4318	4.7	PMN J0327−1529 (4′7)	...	Radio source
52.9615	−61.7174	4.4	IRAS F03305−6158 (5′8)	...	IR source
53.2862	30.9969	8.6	87GB 033012.2+304428 (5′3)	...	Radio source; near Galactic star-forming region
53.7967	−13.9383	4.4	NVSS J033512−135703 (0′8)	...	Radio source
54.7493	−12.5188	4.2	GALEX 2692741389941212225 (3′4)	2.2	Possible quasar
55.0913	−21.3934	5.6	PKS 0338−214 (5′2)	...	FSRQ
59.3980	6.4552	6.4	NVSS J035702+063015 (8′7)	...	Radio source
66.1765	−53.4321	5.3	CRATES J0425−5331 (6′9)	...	FSRQ
67.7599	−60.3547	10.1	ESO 118−G 029 (3′3)	...	S0 galaxy
69.6320	−45.3140	10.7	PKS 0437−454 (6′2)	...	Blazar candidate
72.4882	11.6054	5.5	NVSS J044929+113216 (7′8)	...	Radio source
80.4948	35.7555	5.6	NVSSJ052202+355229 (6′9)	...	Radio source
80.6114	32.9544	5.8	[KLK2001] 940930.26 (6′2)	...	GRB
81.3636	−60.2304	5.4	SUMSS J052542−601341 (1′8)	...	Radio source
84.9618	−54.2098	9.9	PKS 0539−543 (9′9)	...	FSRQ
109.2407	45.4418	5.1	NVSS J071708+452203 (4′7)	...	Radio source
113.6889	50.3033	7.7	CGRaBS J0733+5022 (9′3)	...	FSRQ
117.0590	−16.7764	5.5	PMN J0748−1639 (7′2)	...	Radio source
117.0859	45.1622	4.6	B3 0745+452 (3′8)	3.2	Galaxy of unknown type
117.2098	79.0598	6.3	NVSS J075043+790917 (7′8)	...	FSRQ
118.7230	48.4842	9.1	NVSS J075445+482350 (8′0)	2.4	BL Lac
119.4554	37.7479	4.5	SDSS J075751.73+374554.3 (1′1)	...	Quasar
125.8230	40.6476	8.0	B3 0819+408 (4′8)	...	FSRQ
134.2846	72.0019	5.5	NVSS J085545+720543 (8′5)	...	Radio source
134.4593	−20.0023	6.0	IRAS 08559−1956 (9′1)	...	IR source
134.9916	67.4699	5.0	GALEX 2682537904855582223 (8′1)	...	Possible quasar
135.0210	−44.5387	6.3	2MASX J08595620−4433525 (2′2)	...	IR source
135.4634	67.6414	5.7	NVSS J090038+674223 (8′1)	...	Radio source
138.1924	−20.9321	6.8	RX J0913−2103 (8′1)	...	BL Lac

Table 2—Continued

RA (1)	Dec (2)	Sign. (3)	OptID (4)	BAT? (5)	Comments (6)
139.3315	38.8643	4.7	4C 38.28 (6'5)	...	FR II QSO
142.1210	−20.6005	6.7	PKS J0927−2034 (8'8)	2.7	FSRQ
143.2444	86.2417	6.9	CGRaBS J0929+8612 (3'9)	...	FSRQ
144.8152	−17.4112	8.6	PMN J0939−1731 (7'0)	...	FSRQ
145.1797	−28.5810	5.0	PMN J0940−2829 (10'0)	...	Radio source
147.1646	40.6008	5.0	4C 40.24 (4'8)	...	FSRQ
149.1279	47.3611	6.8	GHO 0953+4738 (3'7)	...	Galaxy cluster
149.5143	−13.7279	5.8	2MASX J09573643−1341492 (6'8)	...	IR source
152.1692	−31.4742	4.4	1RXS J100819.7−312407 (6'2)	...	X-ray source
152.3001	−31.6883	6.2	PKS J1008−3138 (5'1)	...	FSRQ
153.3678	23.2755	5.0	CGCG 123−025 (1'8)	1.6	IR source
154.2732	56.0413	5.0	GALEX 2683382329785717300 (3'4)	...	Possible quasar
154.6427	−31.2356	7.2	PKS J1018−3123 (9'8)	...	FSRQ
156.1451	0.6456	5.5	SDSS J102437.04+003926.0 (0'9)	...	Possible quasar
156.7702	74.6228	7.9	NVSS J102739+744005 (3'5)	...	Radio/IR source
157.7529	74.6584	9.0	NVSS J103122+744158 (2'8)	2.2	FSRQ
161.5354	−29.4379	9.0	TXS 1043−291B (3'7)	...	Radio source with lobes
163.9115	69.9321	10.6	2MASX J10543042+6949207 (8'8)	...	X-ray/IR source
164.7596	2.5005	4.7	PMN J1059+0225 (4'9)	1.0	Radio source
166.0430	81.2678	6.2	3B 940318 (6'6)	...	GRB
166.7367	−36.8196	6.8	ESO 377−G 007 (9'6)	...	Spiral galaxy
171.9033	36.3784	8.8	CGRaBS J1121+3620 (5'0)	2.8	FSRQ
175.4210	61.3633	8.3	EXMS B1146+608 (3'5)	...	X-ray source
178.2468	49.5137	10.2	SDSS J115250.29+493220.4 (2'1)	...	Quasar
183.6555	13.1974	5.0	4C 49.22 (4'1)	...	FSRQ
183.8466	13.0637	5.7	SDSS J121506.93+130558.8 (4'5)	...	BAL QSO
184.1765	18.4032	6.2	CGCG 098−127 (1'5)	...	Elliptical galaxy
184.5352	−10.3535	4.9	2MASX J12181358−1026487 (5'7)	...	IR source
184.6073	−0.5755	5.5	PKS J1217−0029 (8'3)	...	BL Lac
186.1276	24.4276	6.7	NVSS J122437+242452 (1'8)	...	Radio source
186.2145	21.7290	4.8	TXS 1222+220 (2'9)	...	Radio source
191.6873	44.3953	5.8	RBS 1154 (2'8)	1.4	BL Lac
195.3049	33.6781	5.2	FIRST J130115.7+334329 (2'9)	...	Radio source
196.1285	12.0585	7.9	SDSS J130426.15+120245.5 (1'4)	...	Quasar
198.4177	−23.8658	6.1	2MASX J13135485−2354023 (3'9)	...	IR source
203.4901	−38.3668	6.0	2MASX J13340073−3820519 (1'3)	...	IR source
204.4920	−24.0832	4.2	ESO 509−84 (2'6)	...	Spiral galaxy
206.5901	−26.0389	5.6	2MASX J13463183−2602032 (2'3)	...	IR source
207.9203	−29.0735	8.8	PKS J1351−2912 (8'0)	...	Blazar
208.3928	37.5322	6.5	NVSS J135344+373227 (2'1)	...	Radio source
210.0310	−14.7102	6.0	2MASX J14000692−1444062 (1'5)	0.7	Galaxy of unknown type
214.0887	5.9172	4.7	3B 940621 (4'1)	...	GRB
214.1380	13.3386	6.7	PKS 1413+135 (8'3)	...	Radio source
215.0146	−8.6040	6.5	2MASX J14201987−0837228 (4'2)	...	IR source
216.9062	−32.8323	7.9	2MASX J14280087−3256085 (7'9)	...	Spiral galaxy

Table 2—Continued

RA (1)	Dec (2)	Sign. (3)	OptID (4)	BAT? (5)	Comments (6)
218.6920	20.5116	5.1	2MASX J14345111+2030416 (1'2)	1.7	IR source
218.8956	20.3668	6.8	SDSS J143539.93+202405.4 (2'4)	...	Quasar
225.4503	55.8271	7.0	SDSS J150153.53+555309.7 (3'6)	...	Quasar
230.5842	43.5332	5.5	CGRaBS J1521+4336 (7'2)	...	FSRQ
241.5583	85.1381	6.3	NVSS J160701+850215 (6'1)	6.3	Radio source
246.3093	43.6982	4.7	SDSS J162458.54+434036.4 (3'1)	...	Quasar
249.7440	41.5111	5.9	SDSS J163855.92+412937.0 (1'2)	...	Possible quasar
249.8025	39.6816	14.7	SDSS J163851.55+393759.0 (5'0)	...	Quasar
251.1208	−54.6591	4.1	WKK 7381 (4'7)	0.3	Galaxy of unknown type with bright nucleus
252.5771	8.5271	5.5	CGRaBS J1650+0824 (8'2)	...	FSRQ
254.3308	48.2426	14.4	4C 48.41 (7'6)	3.1	FSRQ
254.6441	−1.4666	5.0	PMN J1659−0127 (6'8)	...	Radio source
255.2459	39.8811	4.2	FIRST J170108.8+395443 (2'7)	0.2	BL Lac
259.3781	68.6269	9.0	VII Zw 707 (5'8)	...	IR source

Note. — Col.(1): Right ascension in degrees. Col.(2): Declination in degrees. Col.(3): *Fermi*/LAT detection significance. Col.(4): Most likely optical counterpart within 10 arcminutes of the nominal position. The value in the parantheses represent the difference between the nominal *Fermi*/LAT position and that of the optical counterpart. Col.(5): Approximate detection significance of the *Fermi*/LAT source by *Swift*/BAT within the *Swift*/BAT position error of 4 arcminutes. Col.(6): Comments about the nature of the optical counterpart to the *Fermi*/LAT source.

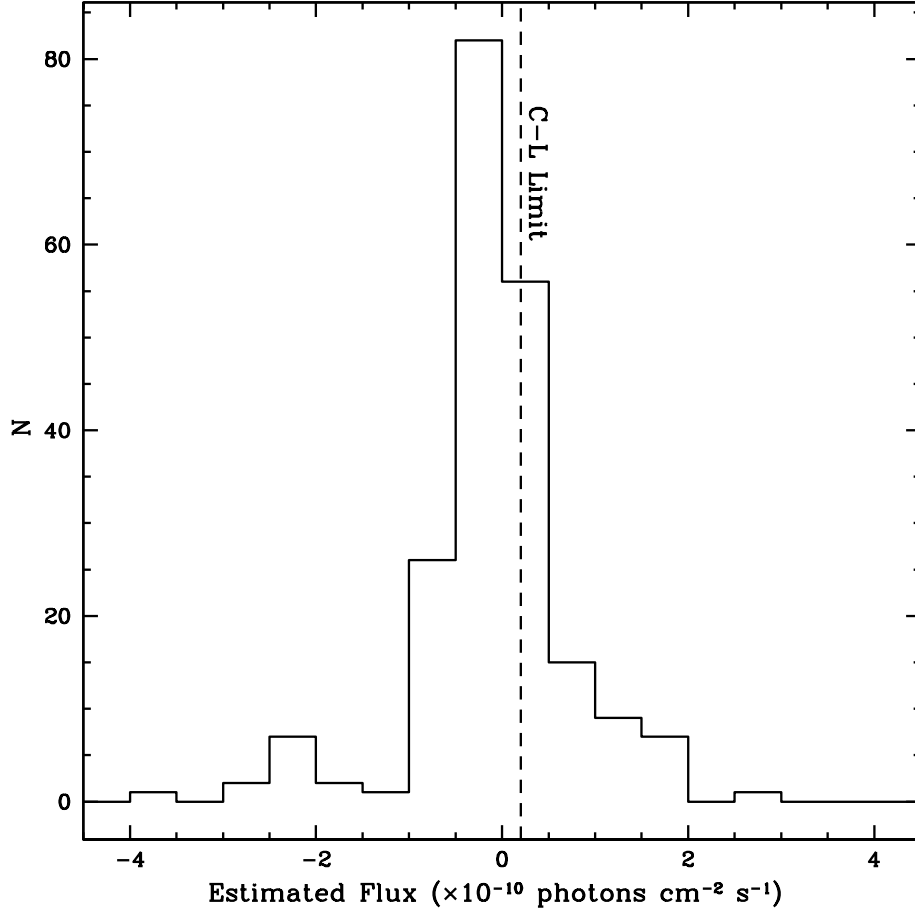


Fig. 1.— Distribution of source fluxes as derived from individual source analysis. These fluxes were derived by assuming point sources at the location of the Seyfert galaxies and a single power law model with  $\Gamma = 2.4$ . The vertical dashed line represents the limit from Composite Likelihood Analysis of 215 BAT Seyferts ( $\sim 2 \times 10^{-11}$  photons  $\text{cm}^{-2} \text{s}^{-1}$ ).



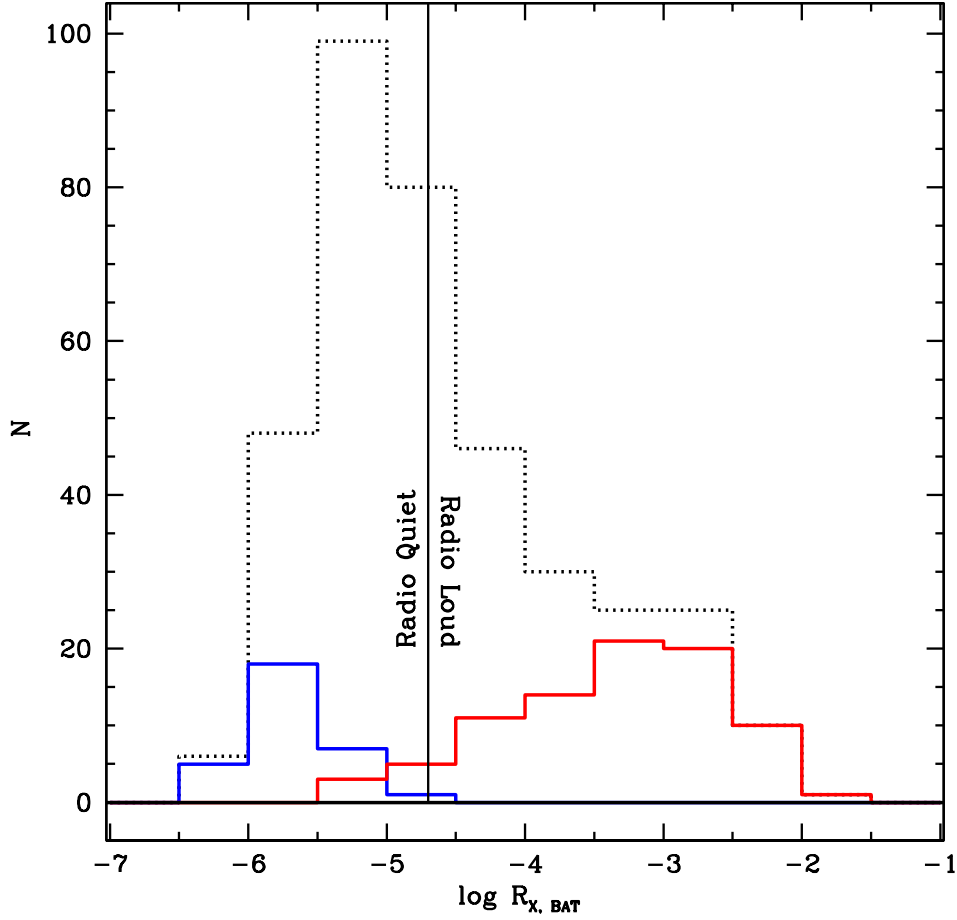


Fig. 2.— Distribution of radio-loudness ( $\log R_{X,BAT}$ ) amongst the extragalactic 58-month *Swift*/BAT sources. The dotted histogram represents all of the extragalactic sources in the *Swift*/BAT sample that have available 1.4 GHz fluxes from FIRST, NVSS, or reliable VLA measurements from the literature (i.e. the parent sample). Although the distribution appears to be skewed toward radio quiet sources, this is uncertain because it depends on the availability of radio data. The blue histogram represents the sub-sample of radio-quiet Seyfert 1s and the red represents that of the sub-sample of blazars and FSRQs identified in the *Swift*/BAT sample. There is a clear distinction between the two classes and that our radio-loudness cutoff is able to separate between the two classes. NGC 1068 and NGC 4945 are very similar to the blazars in terms of radio loudness with  $\log R_{X,BAT}$  of  $-3.7$  and  $-4.3$ , respectively. Nearly all of the radio loud objects have already been identified by *Fermi*.

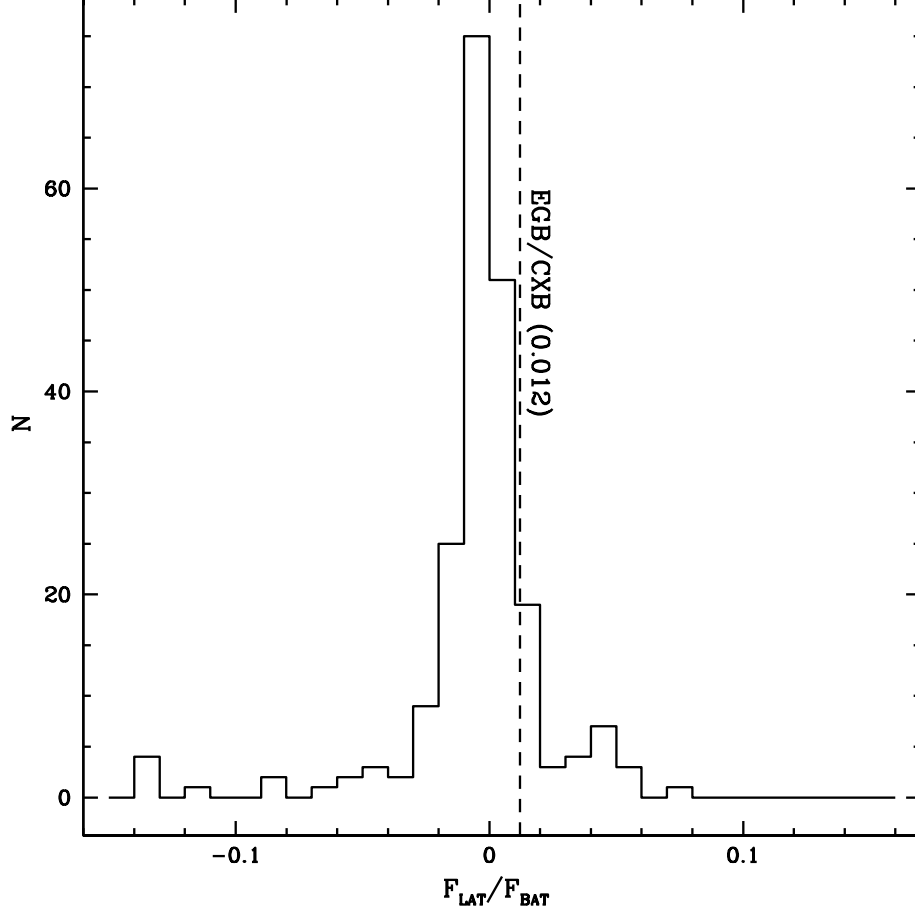


Fig. 3.— Distribution of the upper limits to the  $\gamma$ -to-X-ray flux ratio from individual source analysis. The  $\gamma$ -ray fluxes are those from Figure 1. Assuming no evolution as a function of redshift, the majority of the distribution lies below the EGB/CXB ratio (1.2%). This implies that radio quiet Seyferts are not a source of the EGB. The flux ratio also suggest that radiatively inefficient accretion is not a  $\gamma$ -ray production mechanism in Seyfert galaxies.

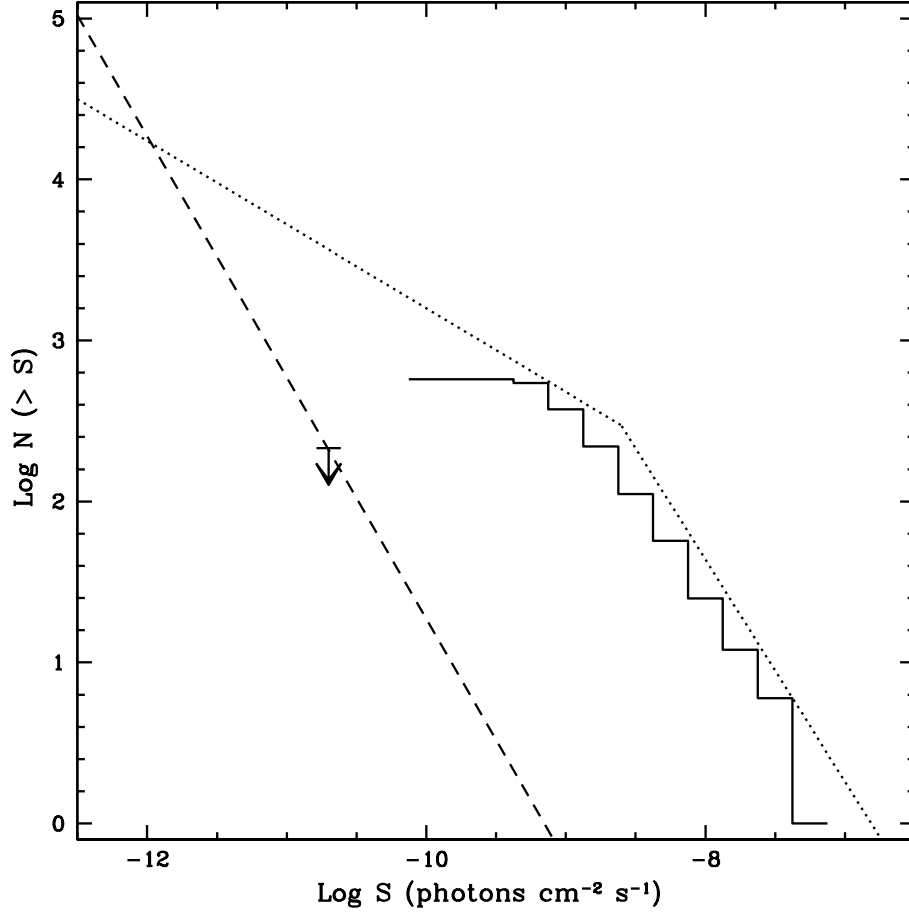


Fig. 4.— Cumulative  $\log N - \log S$  of *Fermi* sources. The histogram represents the distribution of 573 detected objects associated with blazars (BL Lac sources + FSRQs) in the *Fermi* 1-year Catalog. The dotted line is the empirical  $\log N - \log S$  relation derived for these sources in the 1–100 GeV band from Abdo et al. (2010b). There is a break in the power law relation at  $2 \times 10^{-9}$  photons  $\text{cm}^{-2} \text{s}^{-1}$  with a differential power law slope of 2.4 at fluxes above the break and 1.5 below. Also plotted is the upper limit derived from 2.1 years of *Fermi* data on the *Swift*/BAT Seyferts. The dashed line has a differential power law slope of 2.5, assuming the same slope as that found by *Swift* (Ajello et al. 2009) and scaled to intersect the derived upper limit from *Fermi* data (labeled with the arrow). Contributions by Seyfert galaxies would not begin to dominate the EGB until below  $\sim 10^{-12}$  photons  $\text{cm}^{-2} \text{s}^{-1}$ , far below the current sensitivity of *Fermi* data. In order for the integrated flux from the Seyfert galaxies to equal that of the “missing” EGB fraction, the instrument needs to have point source sensitivity  $\lesssim 10^{-23}$  photons  $\text{cm}^{-2} \text{s}^{-1}$ .